Binding and structure-kinetic relationship analysis of selective TLR4-targeted immunosuppressive self-assembling heparin nanoparticles

Hasan Babazada, Shinya Yanamoto, Mitsuru Hashida, Fumiyoshi Yamashita

PII: S0378-5173(18)30709-9
DOI: https://doi.org/10.1016/j.ijpharm.2018.09.054
Reference: IJP 17802

To appear in: *International Journal of Pharmaceutics*

Received Date: 3 August 2018
Revised Date: 18 September 2018
Accepted Date: 20 September 2018

Please cite this article as: H. Babazada, S. Yanamoto, M. Hashida, F. Yamashita, Binding and structure-kinetic relationship analysis of selective TLR4-targeted immunosuppressive self-assembling heparin nanoparticles, *International Journal of Pharmaceutics* (2018), doi: https://doi.org/10.1016/j.ijpharm.2018.09.054

International Journal of Pharmaceutics

Regular Paper

Binding and structure-kinetic relationship analysis of selective TLR4-targeted immunosuppressive self-assembling heparin nanoparticles

Hasan Babazada[a], Shinya Yanamoto[b], Mitsuru Hashida[b,c], Fumiyoshi Yamashita[b*]

[a] Department of Anesthesiology and Critical Care, Perelman School of Medicine, University of Pennsylvania, 3620 Hamilton Walk, Philadelphia, PA 19104, USA

[b] Department of Drug Delivery Research, Graduate School of Pharmaceutical Sciences, Kyoto University, Yoshidashimoadachi-cho, Sakyo-ku, Kyoto 606-8501, Japan.

[c] Institute for Integrated Cell-Material Sciences, Kyoto University, Yoshidaushinomiya-cho, Sakyo-ku, Kyoto 606-8501, Japan.

[*]Corresponding author info:

Tel.: 81-75-753-4525

Fax: 81-75-753-4575

Email: yama@pharm.kyoto-u.ac.jp

Abstract

Self-assembling aliphatic heparin derivatives were shown to inhibit the immune system by antagonizing Toll-like receptor 4/myeloid differentiation protein 2 (TLR4/MD2). In the present study, glycol split heparin–D-erythro-sphingosine conjugates (NAHNP) and its regioselectively desulfated derivatives with shortened aliphatic chains were investigated regarding their biophysical properties in the interaction with TLR4/MD2. Two-dimensional nuclear Overhauser effect spectroscopy studies showed that upon glycol splitting, the heparin backbone gains extra adaptability that facilitates binding to proteins. However, unlike native heparin or glycol split non-anticoagulant heparin (NAH), hydrophobic derivatization of NAH forces sulfated iduronic acid residues to change configuration from a $^{2}S_{0}$ skew-boat to a $^{1}C_{4}$ chair form. Whereas neither heparin nor NAH had any appreciable effect, NAHNP significantly inhibited lipopolysaccharide-induced activation of the NF-κB transcription factor. We showed that NAHNP binds to TLR4/MD2 with an affinity of 62.3 nM. In line with computational studies, biosensor-based structure-kinetic relationship studies demonstrated that 6-O-sulfo groups of D-glucosamine residue were essential in binding to arginines of both TLR4 and MD2 domains of the receptor complex. The desulfation of 6-O-sulfo groups decreases the association kinetics from 4.2×10^{4} M^{-1} s^{-1} to 3.8×10^{3} M^{-1} s^{-1}, which results in a decreased affinity of 800 nM. Two aliphatic chains of NAHNP bound to the MD2 pocket similarly to lipopolysaccharide. A decrease in chain length resulted in a loss of inhibitory activity on NF-κB transcription and binding affinity to TLR4/MD2. In conclusion, the present study characterizes the immunosuppressive effect of aliphatic heparin derivatives and provides a promising strategy to develop selective immunosuppressants for acute and chronic inflammatory disorders.

Keywords

heparin nanoparticles

Toll-like receptor 4

molecular interaction kinetics

surface plasmon resonance

molecular dynamic simulation

nuclear factor kappa B

1. Introduction

Antiinflammatory and immunosuppressive drugs have been indispensable for the management of intolerant immunity in autoimmune diseases, such as rheumatoid arthritis, systemic lupus erythematosus and Crohn's disease (Li et al., 2017). Although many steroidal or nonsteroidal immunosuppressive drugs are currently in use, including corticosteroids, cyclosporin A, tacrolimus, mycophenolic acid, methotrexate, and sirolimus, they simultaneously alter the expression of many genes in a nonspecific multitarget manner (Hartono et al., 2013). As a result, these drugs possess neuro- and nephrotoxicity (Olyaei et al., 2001; Wijdicks, 2001) and also cause general immunodeficiency (Schwartz, 2000).

Identification of the molecular targets of specific pathways responsible for immunosuppression is of therapeutic importance. One of the recent approaches involves designing biomaterials as delivery carriers to narrow the target to immune and inflammatory cells and modulate the immune system (Andorko and Jewell, 2017). Current methods to achieve such immunosuppression include strategies mostly within implantable biomaterials with incorporated or conjugated drugs (Anderson, 2001), modified biomaterial surfaces with nitric oxide-releasing coatings (Mihu et al., 2010) and functionalized biomaterials with growth factors (Leonard and Koria, 2017). Biomaterials themselves also may be intrinsically bioactive because of their architectural properties, such as shape and size, or due to interactions with proteins. Sulfated glycosaminoglycans (GAG) such as heparin and heparan sulfate have been reported to bind to proteins such as cytokines and growth factors and to positively (Borghesi et al., 1999; Yayon et al., 1991) or negatively (Däubener et al., 1995; Rashidiani et al., 2017; Rix et al., 1997; Salek-Ardakani et al., 2000) modulate immune cells. The orientation and linkage of sulfate groups of heparin, as well as the overall molecular shape, charge, and conformational flexibility of the pyranose ring of iduronate residue, play an important role in specificity of protein binding (Mulloy and Forster, 2000). We have previously shown that when heparin and its non-anticoagulant derivatives gain a strong immunosuppressive effect *in vitro* and *in vivo* when they hydrophobically are modified with aliphatic lipid chains (Babazada et al., 2014; Yanamoto et al., 2017) (H. Babazada et al., 2014). These amphiphilic derivatives can self-assemble in water and form nanoparticles of 100-150 nm. We showed that these derivatives could inhibit the lipopolysaccharide-induced production of proinflammatory cytokines by antagonizing the Toll-like receptor 4/myeloid differentiation protein 2 (TLR4/MD2). However, the biophysical basis of interaction between amphiphilic heparin derivatives and TLR4/MD2 complex remains unclear.

Here, we employed nuclear magnetic resonance spectroscopy (NMR) first to characterize the structure of these derivatives and then the surface plasmon resonance (SPR) technique to determine the affinity and kinetics of the interaction with TLR4/MD2. Moreover, we used amphiphilic heparin derivatives with modified sulfation patterns and hydrophobic chains to investigate the structure-kinetic relationship of binding and its impact on functional activity on suppressing the nuclear factor kappa B (NF-κB) transcription factor. Finally, we performed NMR-guided docking and molecular dynamics simulation analysis to investigate the participating residues of TLR4/MD2 and pharmacophore groups of amphiphilic heparin derivatives in binding.

2. Materials and Methods

2.1. Synthesis of heparin derivatives

Heparin (MW 15 kDa; Nacalai Tesque, Inc., Kyoto, Japan) was periodate oxidized at 4 °C, pH 4.0 for 72 h, and borohydride reduced to receive a glycol split non-anticoagulant heparin (NAH), as described previously (Conrad and Guo, 1992). Amphiphilic NAH derivatives were synthesized by conjugating NAH with D-erythro-sphingosine (LKT Laboratories, Inc., St. Paul, MN), 1-octadecanamine, 1-decanamine, and 1-pentanamine to obtain NAHNP, NAHOCT, NAHDEC and NAHPEN, respectively, as described previously (Hasan Babazada et al., 2014). Additionally, 2-O-desulfated, 6-O-desulfated and N-desulfated re-N-acetylated heparins were prepared as reported previously (Babazada et al., 2014). Resulting desulfated derivatives of heparin then were periodate oxidized and borohydride reduced and linked with D-erythro-sphingosine via carboxylic groups of each product to synthesize 2-ODSNP, 6-ODSNP and NDSNP, respectively. To purify heparin conjugates, reaction mixtures were precipitated in pure ethanol, centrifuged 14,000 ×g for 10 min followed by decantation. This was repeated 3 times to remove any remaining unreacted aliphatic amines and reaction solutions. Precipitates were then dried in a vacuum and lyophilized.

2.2. Transient transfection and NF-κB reporter assay

NF-κB reporter constructs were obtained from SABiosciences (Frederick, MD) as a dual luciferase Signal Reporter Assay Kit. The reporter contained a mixture of inducible transcription factor responsive firefly luciferase gene under the control of a basal promoter element (TATA) and constitutively expressing Renilla luciferase gene linked to CMV promoter. Constructs containing a mixture of constitutively expressing green fluorescent protein (GFP), firefly luciferase and Renilla luciferase linked to a CMV promoter were used as a positive control. A mixture of non-inducible firefly luciferase reporter and constitutively expressing Renilla constructs was used as a negative control. For the reporter assay, RAW 264.7 cells were seeded into 24-well plates at a density of 4×10^5 cells per well in 500 µL of Opti-MEM I containing 5% of fetal bovine serum (FBS). The cells were transfected transiently with 100 ng of plasmids (reporter, positive, or negative control) for 72 h using Lipofectamine 3000 reagent (Thermo Fisher Scientific Inc., Pittsburgh, PA), according to the manufacturer's procedures. The cells were washed with PBS after transfection and treated with LPS (20 ng/mL) with or without test compounds at a final concentration of 0.1 mg/mL. Cells were lysed 6 h after stimulation and luciferase activities were measured using PicaGene® Luminescence Kit (Toyo Ink Manufacturing Co., Ltd., Tokyo, Japan) reagents, following the manufacturer's instructions. All samples were pyrogen-free to avoid endotoxin contamination *in vitro*. Endotoxin was tested by gel-clot technique using Limulus ES-II series kit (Wako Pure Chemical Co., Osaka, Japan) according to the manufacturer's instructions.

2.3. NMR spectroscopy

Conjugates were freeze-dried three times in D_2O (99.90 atom %; Euriso-top, Saint-Aubin, France) to remove exchangeable protons prior to NMR measurements. Heparin and NAH were dissolved in D_2O and NAHNP was dissolved in D_2O/ethanol-d_6 (10:1 v/v) at concentrations of 20 mg/mL. NMR experiments were performed at 298 K using a JEOL 500 spectrometer (Jeol Ltd., Tokyo, Japan) operating at an ^1H resonance frequency of 500 MHz. Proton spectra was recorded using a single-pulse program with presaturation of the residual water signal, with the recycle delay of 20 s and 64 transients. The Lorentzian-Gaussian function was applied to enhance the resolution of free induction decay (FID). Chemical shifts

were referenced to internal 3-(trimethylsilyl)-2,2,3,3-tetradeuteropropionic acid (TMSP-d4) signal. Phase-sensitive 2D ^{1}H-^{1}H nuclear Overheuser effect spectroscopy (NOESY) experiments used a $\pi/2$ -t_1 -$\pi/2$- τ_m -$\pi/2$-FID pulse program with 256 t_1 increments and 1024 data points for t_2 accrued with 32 transients. NOE building-up time and relaxation delay were 0.5 s and 1.5 s, respectively. Data were zero-filled and 2D Fourier transformed onto a data matrix of 2K×1K points with phase-shifted sine-bell apodization functions for both dimensions. NOE cross-peaks were classified as very strong, strong, medium and weak, based on their integrated volumes, and assigned an upper bound of distance restraints of 2.7 Å, 3.3 Å, 4.0 Å and 5.0 Å, respectively. Delta NMR Software v 4.3.6 was used for data acquisition and subsequent processing.

2.4. Surface plasmon resonance

SPR experiments were performed using the ProteOn XPR36 Protein Interaction Array System (Bio-Rad Laboratories Inc., Hercules, CA). The ProteOn™ GLH sensor chip was activated with a 5-min injection (150 µL) of solution containing 40 mM N-ethyl-N'-[3-diethylamino-propyl]-carbodiimide (EDC) and 10 mM N-hydroxysulfosuccinimide (sulfo-NHS). Human TLR4/MD2 (5 µg/mL) in 10 mM sodium acetate buffer (pH 5.0) then was injected for 5 min across the activated surface. The remaining active NHS groups were blocked by a 150-µL injection of 1 M ethanolamine in water (pH 8.2). Flow channel 6 was activated and blocked to use as a reference channel. The binding analyses were performed at a flow rate of 60 µL/min at 25 °C in HBS running buffer (10 mM Hepes, 150 mM NaCl, pH 7.4). Following the injection of analytes, the surface was regenerated with a 1-min injection of 10 mM sodium hydroxide. Receptor neutralization was performed by injecting 100 µL of MD2 specific anti-MD2 antibody (ab24182, Abcam, Cambridge, MA) diluted to 30 µg/mL concentration in the running buffer, for 4 min over the immobilized surface before injecting analytes. Double-referenced data were extracted and analyzed using the nonlinear least squares analysis method, as described previously (Oshannessy et al., 1993).

2.5. Structural modeling and molecular dynamics simulation

The 3D structure of pentasaccharide fragment 2-deoxy-2-sulfamido-α-D-glucopyranosyl-3,6-di-*O*-sulfate–β-D-glucuronic acid–2-*O*-sulfo-α-L-iduronic acid–2-deoxy-2-sulfamido-α-D-glucopyranosyl-6-*O*-sulfate ($GlcN_{NS6S}$–GlcA–$GlcN_{NS,3S,6S}$–$IdoA_{2S}$–$GlcN_{NS,6S}$) of NAHNP was generated using GLYCAM-Web GAG builder (www.glycam.org). Configuration of $IdoA_{2S}$ was chosen as $^{1}C_4$ according to the NMR results. The C_2-C_3 bond of GlcA then was cleaved (glycol splitting; gsGlcA) and the structure of D-erythro-sphingosine molecule was attached to the carboxylic groups of gsGlcA and $IdoA_{2S}$, using GaussView 5 (Gaussian, Inc., Pittsburgh, PA). The structure was geometry optimized using the Hartree-Fock method with the 6-31g (d,p) basis set, using Gaussian 09 (Gaussian, Inc., Pittsburgh, PA). The resulting structure of NAHNP was docked to the human TLR4/MD2 receptor (PDB: 3FXI) using AutoDock Vina (Trott and Olson, 2010). Molecular dynamics simulations of NAHNP–TLR4/MD2 complex were performed using Desmond with MPI functionality and periodic boundary conditions (Lindorff-Larsen et al., 2010). The restrained electrostatic potential (RESP) fit model was used to apply partial charges (Bayly et al., 1993). The NAHNP–receptor complex was solvated directly in TIP3P water; sodium and chloride ions were added to the 0.15 M concentration for overall electroneutrality. The ff14SB force field was used for molecular dynamics calculations (Salomon-Ferrer et al., 2013). System underwent 10000

steps of conjugate gradient minimization. The simulation underwent an equilibration with NMR NOE-derived restraints, particularly for $^{1}C_4$ and $^{4}C_1$ configurations of $IdoA_{2S}$ and glucosamine residues respectively, which then were released. Production simulations were performed under NPT conditions at 300 K, with a Langevin piston barostat and Langevin thermostat, and a 2-femtosecond time-step.

2.6. Statistical analysis

One-way analysis of variance was used for in vitro NF-κB activity, and the Tukey's post hoc test was applied when the effect of the factors was significant (GraphPad Prism 7, GraphPad Software Inc., San Diego, CA). Differences at $P < 0.05$ were considered significant.

3. Results and Discussion

3.1. Aliphatic heparin derivatives

Glycol splitting of heparin at 4 °C results in a ring opening of nonsulfated GlcA rings by the cleavage of the C2-C3 bond (Fransson, 1978). This eliminates the anticoagulation properties of heparin and gives additional conformational freedom to the chain within the rigid $GlcN_{NS,6S}$-GlcA-$GlcN_{NS,3S,6S}$ site. This modification preserves heparin's other intrinsic properties, including binding to proteins. Flexibility induced by glycol splitting was also shown to accelerate interaction of heparin with proteins (Casu et al., 2002). We attached D-erythro-sphingosine to the carboxylic groups of this non-anticoagulant heparin (NAH) derivative to synthesize self-assembling nanoparticles of NAH-D-erythro-sphingosine (NAHNP) (Figure 1). Furthermore, different regioselectively desulfated NAH derivatives at 2-O-, N-, and 6-O- positions have been synthesized and conjugated with D-erythro-sphingosine to receive 2ODSNP, NDSNP and 6ODSNP, respectively. The resulting desulfated conjugates were used to analyze the involvement of sulfo groups of NAHNP in binding affinity and kinetics to TLR4/MD2. In addition, to investigate the effect of aliphatic chain length on binding properties, NAH was conjugated to 1-pentanamine (5-carbon atom length), 1-decanamine (10-carbon atom length) and 1-octadecanamine (18-carbon atom length) to receive NAHPEN, NAHDEC and NAHOCT, respectively. Intact heparin was used to synthesize heparin-D-erythro-sphingosine conjugate (HPNP).

3.2. Structural properties of NAHNP

Assignment of the anomeric proton signals in the ^{1}H NMR spectrum of NAH confirmed the glycol splitting with the absence of peaks at 4.61 ppm and 5.01 ppm, characteristic of non-sulfated GlcA and IdoA residues, respectively (Alekseeva et al., 2014), and the absence of the H2 peak of GlcA at 3.36 ppm. NOE enhancements between H3 of gsGlcA and H3 of succeeding $GlcN_{NS,3S,6S}$ were observed (Figure 2A). This NOE cross peak was absent in heparin, as these protons locate in different residues at a more-than 5 Å distance from each other (Figure 2B). These observations suggest that dihedral angles gain more degrees of freedom upon glycol splitting, which gives extra flexibility to the backbone. The $^{3}J_{H\text{-}H}$ coupling constants indicated that glycol splitting did not affect the $^{4}C_1$ configuration of sulfated glucosamine residues. In fact, small $^{3}J_{H1\text{-}H2}$ couplings (< 3.5 Hz) suggest an axial-equatorial relationship, whereas larger values for $^{3}J_{H2\text{-}H3}$ (11.6 Hz), $^{3}J_{H3\text{-}H4}$ (10.02 Hz) and $^{3}J_{H4\text{-}H5}$ (10.45 Hz) indicate a transdiaxial relationship between these protons. It has been

shown that conformation plasticity of the pyranose ring of internal $IdoA_{2S}$ residue in heparin is in equilibrium between two forms, the $^1C_4$ chair and the $^2S_0$ skew-boat (Ferro et al., 1990; Mulloy et al., 1993). Observed $^3J_{H2\text{-}H3}$ (6.6 Hz) and $^3J_{H3\text{-}H4}$ (3.8 Hz) values and ^1H-^1H NOE enhancements for H2-H5 and H1-H3 for both heparin and NAH imply the average of static $^2S_0$ ring configuration for $IdoA_{2S}$ residues. However, ^1H-^1H NOE studies of NAHNP showed that conjugation of D-erythro-sphingosine, forces the internal $IdoA_{2S}$ to adopt a $^1C_4$ configuration (Figure 2C). This was observed by the absence of H2-H5 and enhanced H1-H2 and H4-H5 cross peaks. Moreover, we could observe the NOE enhancement between the proton of C4 of D-erythro-sphingosine (5.52 ppm) and the H4 of $GlcN_{NS,3S,6S}$ (3.70 ppm). Protons of C4 of sphingosine gave also intraresidual cross peaks with nearby protons of C3 (4.20 ppm) and C1 (3.20 ppm). Protons of D-erythro-sphingosine attached to the Ido2S residue also gave cross peaks with this residue (Figure 2C).

3.3. Effect of amphiphilic heparin derivatives on NF-κB activation

NAHNP strongly inhibited the activation of the NF-κB transcription factor in LPS-stimulated macrophages (Figure 3A). HPNP had a smaller antiinflammatory effect than NAHNP, indicating the critical role of C2-C3 glycol splitting of GlcA in antiinflammatory potency. The NF-κB reporter assay revealed that selective desulfation of N-sulfo (at C-2 of the D-glucosamine residues) and 2-O-sulfo (at C-2 of L-iduronic or D-glucuronic acid residues) groups did not affect the inhibitory properties of NAHNP significantly (Figure 3B). In contrast, the removal of 6-O-sulfate groups (at C-6 of D-glucosamine residues) significantly reduced the anti-inflammatory effect, indicating the importance of 6-O-sulfate groups in the potency of NAHNP. Changes in the length of hydrocarbon chains altered the activity of NAHNP. Thus, NAHDEC and NAHPEN (with ten and five carbon atom chains, respectively) showed no inhibitory effect (Figure 3C). Conjugates containing the same 18-carbon length of aliphatic chain as D-erythro-sphingosine, *i.e.,* 1-octadecanamine, retained an inhibitory effect, suggesting the length of chain is the key pharmacophore along with the 6-O-sulfo groups for NF-κB inhibitory activity.

3.4. Structure-kinetic relationship of amphiphilic heparin derivatives

To investigate the structure-kinetic relationship of synthesized aliphatic heparin derivatives, we immobilized TLR4/MD2 onto the sensor surface and tested all compounds with different sulfation patterns and hydrophobic chain lengths. To avoid mass transfer limitations and non-Langmuirian kinetics due to steric hindrance, R_{max} of ~1000 RU was used for TLR4/MD2, which was sufficient for quantification of all analytes. Out of the immobilized total, nearly 100% of TLR4/MD2 preserved functionality. Association and dissociation phases are shown by sensorgrams of resonance units (RUs) as a function of time obtained for NAHNP, after subtraction of the background signal from the control channel (Figure 4A). The dissociation phase first was analyzed to determine the value of the dissociation rate constant, k_{off}, by fitting the double referenced data to the integrated rate equation

$$R_t = R_a e^{-k_{off} t},$$

where R_t is the response at time t, and R_a is the amplitude of the dissociation process. The obtained k_{off} then was used to estimate the association rate constant, k_{on}, by fitting the association phase data to

$$R = [A]k_{\mathrm{on}}R_{\mathrm{max}}\left[1 - e^{-(([A]k_{\mathrm{on}}+k_{\mathrm{off}})t)}\right]/[[A]k_{\mathrm{on}} + k_{\mathrm{off}}],$$

where [A] is the concentration of the analyte compound, and R_{max} is the maximal response. The affinity was calculated from K_D=k_{off}/k_{on}. The association and dissociation rate constants of NAHNP–TLR4/MD2 binding were 4.2×10^4 M^{-1} s^{-1} and 2.58×10^{-3} s^{-1}, respectively, and the calculated affinity was 62.3 nM at 25 °C. The TLD4/MD2-specific agonist LPS bound to the receptor with a lower affinity of 79 nM, which was consistent with previous studies (74 nM) (Viriyakosol et al., 2000). Although the association rate of LPS, 4.9×10^4 M^{-1} s^{-1}, was compatible to that of the NAHNP dissociation rate, 3.9×10^{-3} s^{-1} was faster (Figure 4B). Injecting the neutralizing anti-MD2 antibodies over the immobilized surface prior to injecting the NAHNP and LPS prevented the binding of both compounds, indicating that NAHNP specifically interacted with the LPS-binding MD2 domain of the receptor complex (Figure 4B).

Selective desulfation of N-sulfo (at C-2 of the D-glucosamine residues) reduced its binding affinity to 130 nM (Figure 4C). The decrease in affinity mainly was due to the decrease in the association rate constant (2.38×10^4 M^{-1} s^{-1}). The desulfation of the N-sulfo groups did not affect the dissociation rate (3.12×10^{-3} s^{-1}) when compared to NAHNP. Removal of the 2-O-sulfo groups (at C-2 of L-iduronic or D-glucuronic acid residues) also decreased the binding affinity (122 nM), which was similar to the N-desulfated derivative. Similar changes in kinetics were observed upon removal of the 2-O-sulfo groups with association and dissociation rates of 2.0×10^4 M^{-1} s^{-1} and 2.43×10^{-3} s^{-1}, respectively. Elimination of the 6-O-sulfate groups (at C-6 of D-glucosamine residues) remarkably reduced the association kinetics (3.8×10^3 M^{-1} s^{-1}) but did not affect the dissociation kinetics (3.02×10^{-3} s^{-1}), indicating that all sulfo groups mainly contribute to the association phase of the interaction, 6-O-sulfate groups being the most prominent. The removal of 6-O-sulfate groups resulted in the dramatic decrease of affinity (800 nM) to the receptor. The binding affinity of NAHNP to the TLR4/MD2 was proportional to the length (*i.e.,* hydrophobicity) of the attached aliphatic chain (Figure 4D). NAHPEN (5-carbon atom length) exhibited no detectable binding compared to NAHDEC (10-carbon atom length). NAHDEC bound to the receptor with a reduced affinity of 1.86 μM with the association and dissociation rates of 5.8×10^3 M^{-1} s^{-1} and 0.01 s^{-1}, respectively. Binding of NAHOCT (18-carbon atom length) to the receptor was similar to NAHNP with affinity, association and dissociation rates of 82 nM, 5.5×10^4 M^{-1} s^{-1} and 4.61×10^{-3} s^{-1}, respectively. Native heparin or NAH failed to bind to the immobilized receptor, indicating the critical pharmacophore role of hydrophobic patterns in recognition by TLR4/MD2. HPNP also had a lower affinity of 520 nM than that of NAHNP, indicating the critical role of the ring opening of nonsulfated glycuronic acid residues in the strength of binding (Figure 4D). This low affinity was the result of the dramatic decrease of association kinetics (6.9×10^3 M^{-1} s^{-1}). Similar to desulfation, glycol splitting did not affect the dissociation kinetics of the interaction (3.65×10^{-3} s^{-1}).

3.5. Binding prediction of NAHNP–TLR4/MD2 interactions using NMR-guided docking and molecular dynamics simulation

We docked NAHNP in vacuo to the TLR4/MD2 complex using AutoDock Vina to obtain energetically reasonable structures of the NAHNP–TLR4/MD2 complex that incorporate NOE-derived constraints and to provide a starting point for a more precise structural fit for

MD in water. Structural modeling was guided by NMR results. Geometry optimization of $GlcN_{NS,6S}$–gsGlcA–$GlcN_{NS,3S,6S}$–$IdoA_{2S}$–$GlcN_{NS,6S}$ at HF/6-31g(d,p) levels revealed the change of dihedral angle $\Psi_{C2\text{-}C1\text{-}O\text{-}C5}$ of gsGlcA from -64 to -171 degrees and $\phi_{O\text{-}C1\text{-}O\text{-}C5}$ from 174 to 67 degrees, bringing H3 of glycol-split GlcA and H3 of $GlcN_{NS,3S,6S}$ closer to 3.39 Å, which resulted in NOE enhancement. However, the H3-H3 distance of gsGlcA and $GlcN_{NS,3S,6S}$ shifted away from each other to 6.12 Å in NAHNP after the attachment of D-erythro-sphingosine. Because NOE intraresidual cross peaks revealed that the IdoA2S residue of NAHNP was in the $^1C_4$ configuration, we restricted this residue during docking. However, distant constrains were lifted and allowed to rotate freely during MD simulations in water to monitor the conformational changes that might result from the interactions with protein. The root mean square deviation (RMSD) analyses indicated that the NAHNP-MD2 complex was stable during the entire duration of the MD run with all alpha carbon RMSD of 2.3 Å (Figure 5A). Residues toward the termini tails for both TLR4 (aa 27-627) and MD2 (aa 19-159) fluctuated the most. The root mean square fluctuations (RMSF) were high for Thr84 and Met85 of MD2, which reside in the unstructured part of the protein, with an RMSF of 3.7 Å and 3.2 Å, respectively (Figure 5A). NAHNP bound to a hydrophobic pocket in human MD2 in a similar way to LPS (Figure 5B). The diglucosamine backbone of NAHNP is exposed to the solvent and aligns parallel to the TLR4 domain. As determined from NMR spectroscopy of NAHNP, sulfated glucosamine residues remained in their $^4C_1$ configuration during the course of MD simulations with the receptor. NOE enhancements for NAHNP revealed that conjugation of D-erythro-sphingosine forces the $IdoA_{2S}$ to adopt a $^1C_4$ configuration unlike both heparin and NAH in which the ring is in average of static $^2S_0$ configuration. MD simulations showed that $IdoA_{2S}$ remained in its $^1C_4$ configuration during the interaction with the receptor. It appeared that glycol splitting resulted in exposed 6-O-sulfo groups toward the TLR4 backbone and formed a direct salt bridge with Asp294 that could contribute to the elevated affinity of NAHNP to the receptor as compared to LPS. This was consistent with the results of SPR as the removal of 6-O-sulfo groups resulted in remarkable decrease of affinity of NAHNP from 62.3 to 800 nM. The N-and 2-O-sulfo groups interacted with Glu92, Ser120 of MD2, and Thr319 and Thr296 of TLR4, respectively. However, water molecules momentarily start to bridge the interactions between donating oxygen atoms of both the N- and 2-O-sulfo groups and the side chain residues, confirming the critical role of 6-O-sulfo groups in binding (Figure 5B). D-erythro-sphingosine chains form hydrophobic interactions with Val135, Leu61, Phe147, Ile117, Ile63, Phe76, Leu78, Phe121, Phe119, Leu54, Ile153, Ile52, Ile32, Val48, Val24, Phe151, Cys133, Ile80 and Ile 124 residues of the MD2 domain. The structure formed by the two acyl chains of NAHNP explores the shape of the hydrophobic pocket, leaving only a narrow channel near its opening. Both aliphatic chains adopt an extended conformation (Figure 5C and D).

4. Conclusion

We show that glycol split heparin conjugated with aliphatic chains selectively bind to TLR4/MD2 with high affinity and suppress the NF-κB transcription factor. Biosensor-based structure-kinetic relationship analysis using regioselectively desulfated heparin derivatives, as well as computational studies, revealed that 6-O-sulfo groups are involved directly in binding strength, loss of which results in reduced association kinetics and affinity. However, sulfo groups do not affect the dissociation kinetics. The length of aliphatic chains of attached

hydrophobic moiety is the key to the binding directly to the MD-2 pocket. A decrease of chain length results in loss of biological effect and remarkably decreases binding affinity.

Acknowledgements

This work was financially supported in part by JSPS KAKENHI under grant numbers JP16H01861(MH), 15K08071(FY), and 18H03531(FY), and the Research on Development of New Drugs from Japan Agency for Medical Research and Development, AMED (FY), and Cosmetology Research Foundation (FY).

Conflict of interest

Authors declare no conflict of interest.

References

Alekseeva, A., Casu, B., Cassinelli, G., Guerrini, M., Torri, G., Naggi, A., 2014. Structural features of glycol-split low-molecular-weight heparins and their heparin lyase generated fragments. Anal. Bioanal. Chem. 406, 249–265. https://doi.org/10.1007/s00216-013-7446-4

Anderson, J.M., 2001. Biological Responses to Materials. Annu. Rev. Mater. Res. 31, 81–110. https://doi.org/10.1146/annurev.matsci.31.1.81

Andorko, J.I., Jewell, C.M., 2017. Designing biomaterials with immunomodulatory properties for tissue engineering and regenerative medicine. Bioeng. Transl. Med. 2, 139–155. https://doi.org/10.1002/btm2.10063

Babazada, H., Yamashita, F., Hashida, M., 2014. Suppression of experimental arthritis with self-assembling glycol-split heparin nanoparticles via inhibition of TLR4-NF-κB signaling. J. Control. Release 194. https://doi.org/10.1016/j.jconrel.2014.09.015

Babazada, H., Yamashita, F., Yanamoto, S., Hashida, M., 2014. Self-assembling lipid modified glycol-split heparin nanoparticles suppress lipopolysaccharide-induced inflammation through TLR4–NF-κB signaling. J. Control. Release 194, 332–340.

Bayly, C.I., Cieplak, P., Cornell, W., Kollman, P.A., 1993. A well-behaved electrostatic potential based method using charge restraints for deriving atomic charges: the RESP model. J. Phys. Chem. 97, 10269–10280. https://doi.org/10.1021/j100142a004

Borghesi, L.A., Yamashita, Y., Kincade, P.W., 1999. Heparan sulfate proteoglycans mediate interleukin-7-dependent B lymphopoiesis. Blood 93, 140–8.

Casu, B., Guerrini, M., Naggi, A., Perez, M., Torri, G., Ribatti, D., Carminati, P., Giannini, G., Penco, S., Pisano, C., Belleri, M., Rusnati, M., Presta, M., 2002. Short heparin sequences spaced by glycol-split uronate residues are antagonists of fibroblast growth factor 2 and angiogenesis inhibitors. Biochemistry 41, 10519–28.

Conrad, H.E., Guo, Y., 1992. Structural analysis of periodate-oxidized heparin. Adv. Exp. Med. Biol. 313, 31–36.

Däubener, W., Nockemann, S., Gutsche, M., Hadding, U., 1995. Heparin inhibits the antiparasitic and immune modulatory effects of human recombinant interferon-gamma. Eur. J. Immunol. 25, 688–92. https://doi.org/10.1002/eji.1830250309

Ferro, D.R., Provasoli, A., Ragazzi, M., Casu, B., Torri, G., Bossennec, V., Perly, B., Sinaÿ, P., Petitou, M., Choay, J., 1990. Conformer populations of l-iduronic acid residues in glycosaminoglycan sequences. Carbohydr. Res. 195, 157–167. https://doi.org/10.1016/0008-6215(90)84164-P

Fransson, L.-Å., 1978. Periodate oxidation of the d-glucuronic acid residues in heparan sulphate and heparin. Carbohydr. Res. 62, 235–244. https://doi.org/10.1016/S0008-6215(00)80870-8

Hartono, C., Muthukumar, T., Suthanthiran, M., 2013. Immunosuppressive drug therapy. Cold Spring Harb. Perspect. Med. 3, a015487. https://doi.org/10.1101/cshperspect.a015487

Leonard, A., Koria, P., 2017. Growth factor functionalized biomaterial for drug delivery and tissue regeneration. J. Bioact. Compat. Polym. 32, 568–581. https://doi.org/10.1177/0883911517705403

Li, P., Zheng, Y., Chen, X., 2017. Drugs for Autoimmune Inflammatory Diseases: From Small Molecule Compounds to Anti-TNF Biologics. Front. Pharmacol. 8, 460. https://doi.org/10.3389/fphar.2017.00460

Lindorff-Larsen, K., Piana, S., Palmo, K., Maragakis, P., Klepeis, J.L., Dror, R.O., Shaw, D.E., 2010. Improved side-chain torsion potentials for the Amber ff99SB protein force field. Proteins 78, 1950–8. https://doi.org/10.1002/prot.22711

Mihu, M.R., Sandkovsky, U., Han, G., Friedman, J.M., Nosanchuk, J.D., Martinez, L.R., 2010. The use of nitric oxide releasing nanoparticles as a treatment against *Acinetobacter baumannii* in wound infections. Virulence 1, 62–67. https://doi.org/10.4161/viru.1.2.10038

Mulloy, B., Forster, M.J., 2000. Conformation and dynamics of heparin and heparan sulfate. Glycobiology 10, 1147–56.

Mulloy, B., Forster, M.J., Jones, C., Davies, D.B., 1993. N.m.r. and molecular-modelling studies of the solution conformation of heparin. Biochem. J. 293 (Pt 3), 849–58. https://doi.org/10.1042/BJ2930849

Olyaei, A.J., de Mattos, A.M., Bennett, W.M., 2001. Nephrotoxicity of immunosuppressive drugs: new insight and preventive strategies. Curr. Opin. Crit. Care 7, 384–9.

Oshannessy, D.J., Brighamburke, M., Soneson, K.K., Hensley, P., Brooks, I., 1993. Determination of Rate and Equilibrium Binding Constants for Macromolecular Interactions Using Surface Plasmon Resonance: Use of Nonlinear Least Squares Analysis Methods. Anal. Biochem. 212, 457–468.

Rashidiani, S., Jalili, A., Babaei, E., Sheikhesmaeili, F., Fakhari, S., Ataee, P., Parhizkar, B., 2017. The chemokine CCL28 is elevated in the serum of patients with celiac disease and decreased after treatment. Am. J. Clin. Exp. Immunol. 6, 60–65.

Rix, D.A., Douglas, M.S., Leon, M.P., Ali, S., Talbot, D., Kirby, J.A., 1997. Endothelial cells: heparin modulates the induction of functional antigen presentation by IFN-gamma. Biochem. Soc. Trans. 25, 195S.

Salek-Ardakani, S., Arrand, J.R., Shaw, D., Mackett, M., 2000. Heparin and heparan sulfate bind interleukin-10 and modulate its activity. Blood 96, 1879–88.

Salomon-Ferrer, R., Case, D.A., Walker, R.C., 2013. An overview of the Amber biomolecular simulation package. Wiley Interdiscip. Rev. Comput. Mol. Sci. 3, 198–210. https://doi.org/10.1002/wcms.1121

Schwartz, R.S., 2000. Immunodeficiency, Immunosuppression, and Susceptibility to Neoplasms. JNCI Monogr. 2000, 5–9. https://doi.org/10.1093/oxfordjournals.jncimonographs.a024257

Trott, O., Olson, A.J., 2010. AutoDock Vina: improving the speed and accuracy of docking with a new scoring function, efficient optimization, and multithreading. J. Comput. Chem. 31, 455–61. https://doi.org/10.1002/jcc.21334

Viriyakosol, S., Mathison, J.C., Tobias, P.S., Kirkland, T.N., 2000. Structure-function analysis of CD14 as a soluble receptor for lipopolysaccharide. J. Biol. Chem. 275, 3144–9. https://doi.org/10.1074/JBC.275.5.3144

Wijdicks, E., 2001. Neurotoxicity of immunosuppressive drugs. Liver Transplant. 7, 937–942. https://doi.org/10.1053/jlts.2001.27475

Yanamoto, S., Babazada, H., Sakai, S., Higuchi, Y., Yamashita, F., Hashida, M., 2017. Anti-inflammatory effect of self-assembling glycol-split glycosaminoglycan-stearylamine conjugates in lipopolysaccharide-stimulated macrophages. Biol. Pharm. Bull. 40. https://doi.org/10.1248/bpb.b16-00928

Yayon, A., Klagsbrun, M., Esko, J.D., Leder, P., Ornitz, D.M., 1991. Cell surface, heparin-like molecules are required for binding of basic fibroblast growth factor to its high affinity receptor. Cell 64, 841–848. https://doi.org/10.1016/0092-8674(91)90512-W

Figure legends

Figure 1. Synthesis scheme and **structure of NAH derivatives.** Reaction scheme of pentasaccharide $GlcN_{NS,6S}$–gsGlcA–$GlcN_{NS,3S,6S}$–$IdoA_{2S}$–$GlcN_{NS,6S}$ fragment of heparin attached to the hydrophobic moieties is shown. Ψ and ϕ are the dihedral angles of gsGlcA and glycosidic linkages, which are defined as $\Psi_{C2\text{-}C1\text{-}O\text{-}C5}$ and $\phi_{O\text{-}C1\text{-}O\text{-}C5}$. The binding atom of aliphatic chains is shown as x.

Figure 2. The two-dimensional ^{1}H NMR spectra. The NOESY spectra of NAH (A), heparin (B) and NAHNP (C) were measured at 25 °C with a mixing time of 500 ms.

Figure 3. Effect of heparin derivatives on NF-κB signaling activity. Effect of glycol splitting (A), 2-ODSNP, N-DSNP, 6-ODSNP (B), NAHDEC, NAHPEN and NAHOCT (C) on NF-κB transcription activity induced by LPS. RAW264.7 cells (4×10^5 cells per well) were transfected with NF-κB reporter, negative control, and positive control and stimulated with LPS (20 ng/mL) with or without chemically modified heparin derivatives (0.1 mg/mL) for 6 h. Dual-luciferase assays were performed. Reporter activity values are expressed as arbitrary units using a Renilla reporter for internal normalization. Data represent the average ± standard deviation of triplicate samples. $*P < 0.05$, $**P < 0.01$ *vs* LPS.

Figure 4. Surface plasmon resonance of binding of heparin derivatives to human TLR4/MD2 complex. NAHNP (A) was injected at concentrations ranging from 0.0625 to 1 μM over the captured TLR4/MD2 surface at 25 °C. Surface neutralization was performed by flowing an anti-MD2 antibody before injecting NAHNP or LPS at a 1-μM concentration (B). Regioselectively desulfated NDSNP, 2ODSNP and 6ODSNP were injected at a 1-μM concentration to evaluate the effect of sulfo groups on binding (C). Heparin, NAH and derivatives with different aliphatic chain lengths were injected at 1 μM over the immobilized receptor. Kinetic data were extracted using the nonlinear least squares method. K_D was calculated from k_{off}/k_{on}.

Figure 5. Structure of the NAHNP-TLR4/MD-2 Complex. (A) The RMSD of backbone atom positions (top) and fluctuations of local residues (bottom) for NAHNP-TLR4/MD2 at temperature of 25 °C. (B) Capture of NAHNP (red) in the MD2-binding pocket from MD simulations superimposed with LPS (blue) and a detailed schematic of NAHNP-TLR4/MD2 interactions. Colors of circles indicate the interaction type as follows: green, hydrophobic; red, charged; and blue, polar. (C) The overall structure of the NAHNP-TLR4/MD-2 complex. (D) Surface representation of MD2. The TLR4 part of the receptor is colored gray. Positively and negatively charged surfaces are colored blue and red, respectively. Aspartic and glutamic acids interacting ionically with 6-O-sulfo groups of NAHNP are labeled.

Figure 1

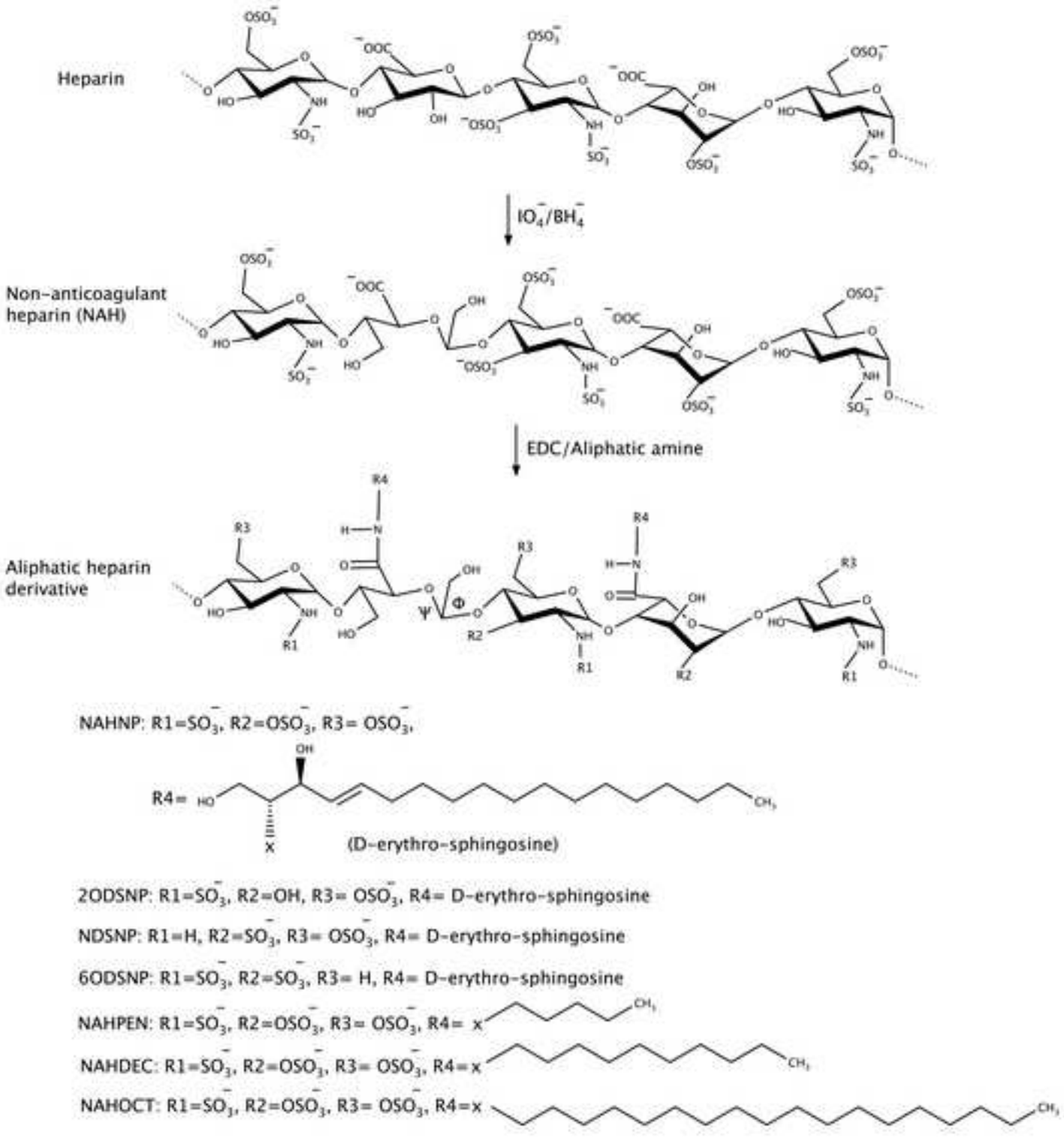

Figure 2

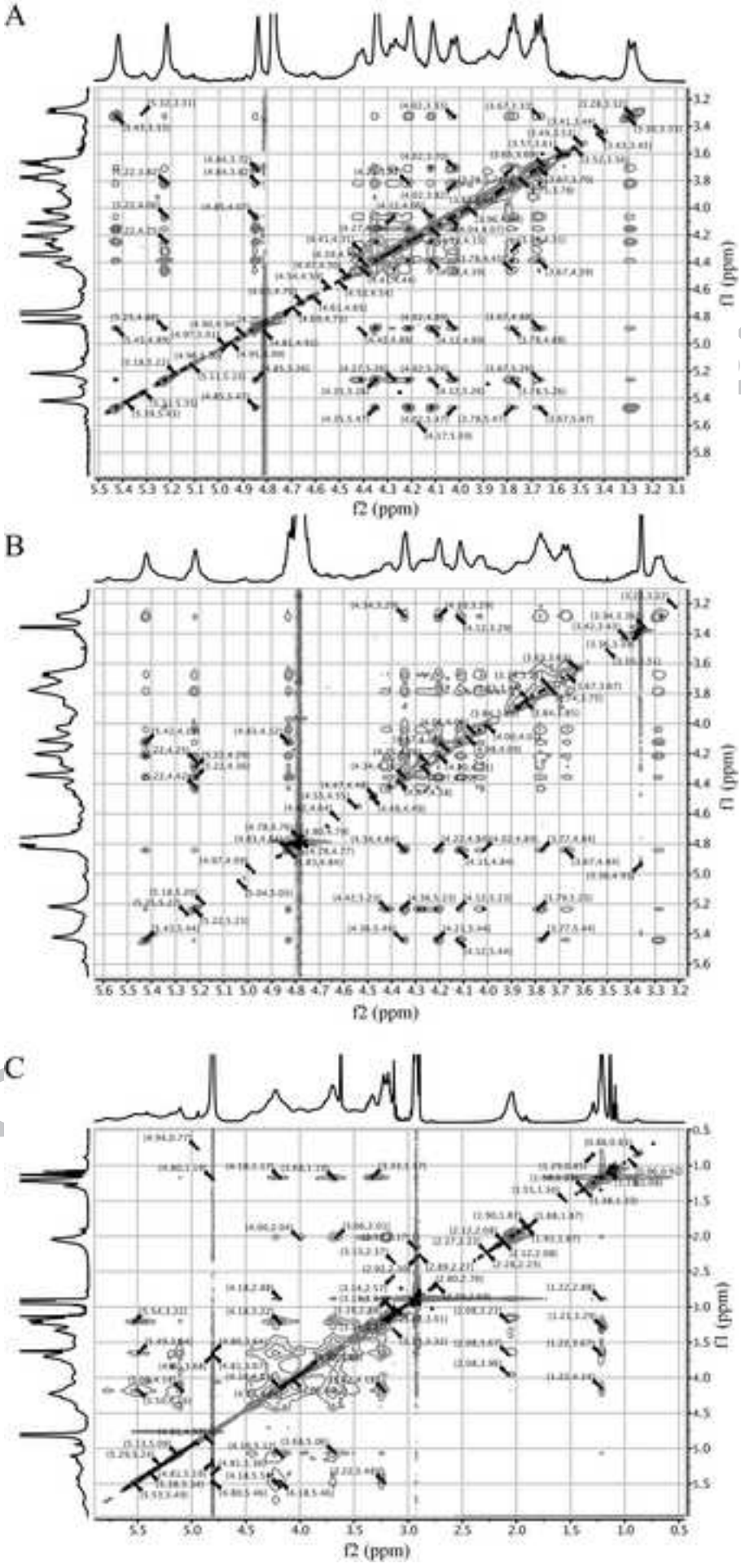

Figure 3

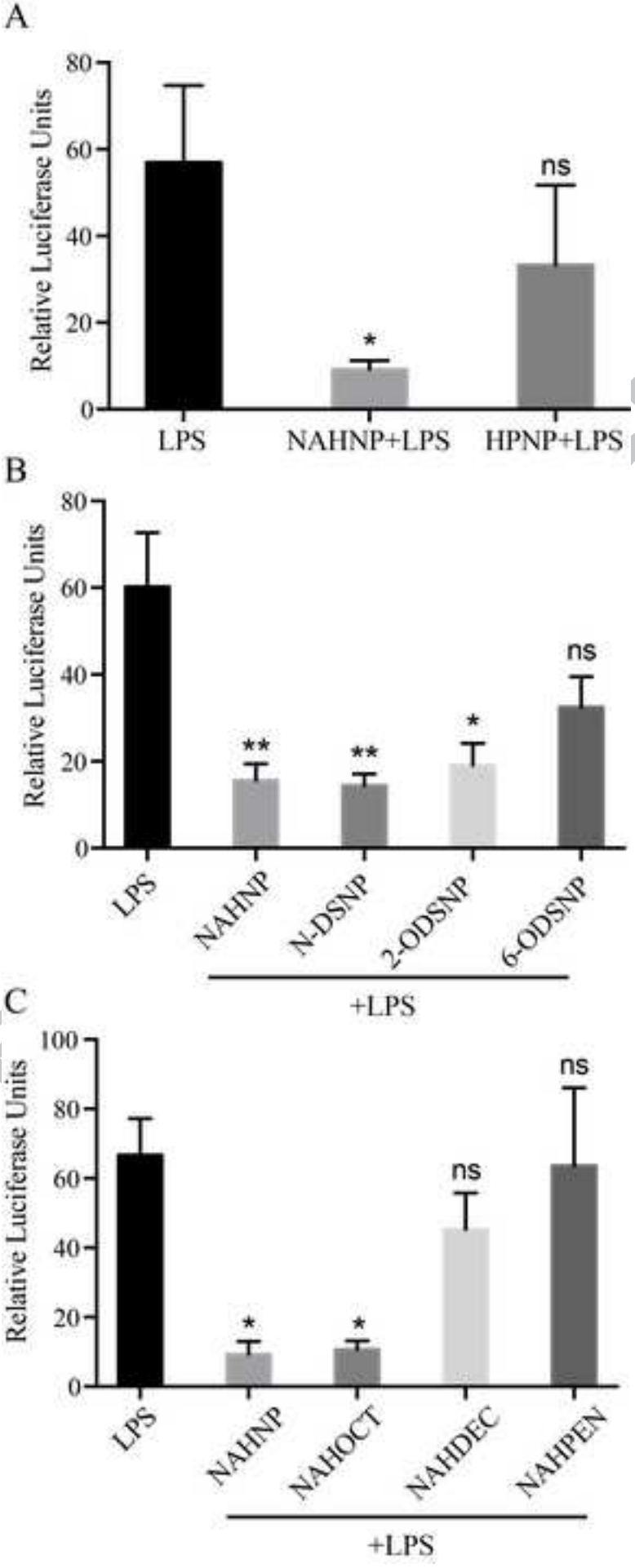

Figure 4

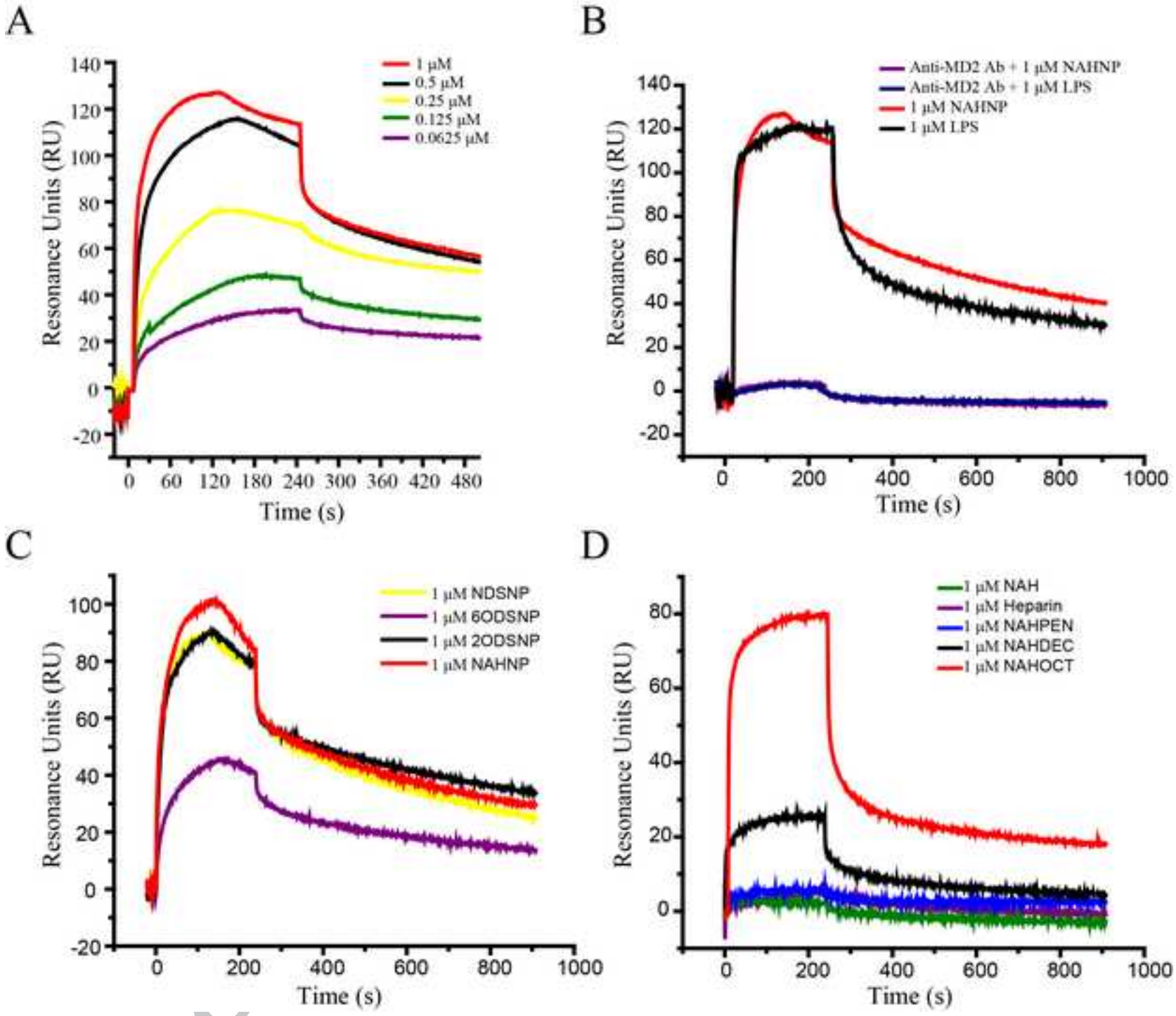

Figure 5

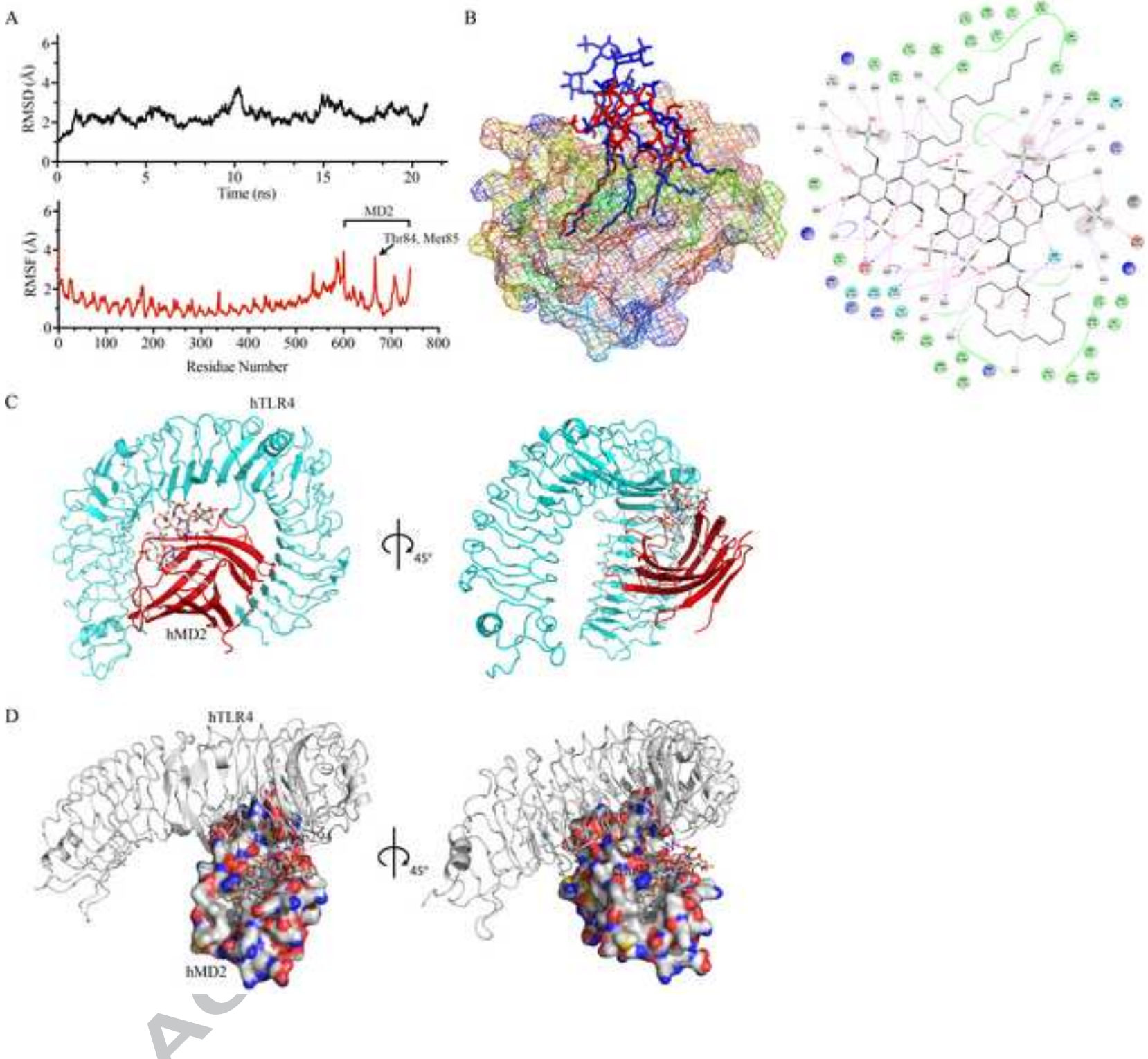

Graphical abstract